A pH-Neutral, Aqueous Redox Flow Battery with a 3600-Cycle Lifetime: Micellization-Enabled High Stability and Crossover Suppression

Jingchao Chai[+],[a] Xiao Wang[+],[a] Amir Lashgari,[a] Caroline K. Williams,[a] and Jianbing (Jimmy) Jiang*[a]

Redox-flow batteries (RFBs) are a highly promising large-scale energy storage technology for mitigating the intermittent nature of renewable energy sources. Here, the design and implementation of a micellization strategy in an anthraquinone-based, pH-neutral, nontoxic, and metal-free aqueous RFB is reported. The micellization strategy (1) improves stability by protecting the redox-active anthraquinone core with a hydrophilic poly(ethylene glycol) shell and (2) increases the overall size to mitigate the crossover issue through a physical blocking mechanism. Paired with a well-established potassium ferrocyanide catholyte, the micelle-based RFB displayed an excellent capacity retention of 90.7% after 3600 charge/discharge cycles (28.3 days), corresponding to a capacity retention of 99.67% per day and 99.998% per cycle. The mechanistic studies of redox-active materials were also conducted and indicated the absence of side reactions commonly observed in other anthraquinone-based RFBs. The outstanding performance of the RFB demonstrates the effectiveness of the micellization strategy for enhancing the performance of organic material-based aqueous RFBs.

Introduction

The rapid development of solar and wind as renewable energy sources has stimulated intense research effort for the development of a sustainable and environmentally-friendly method to mitigate the intermittency of solar and wind power production.[1] Among the several promising energy storage techniques, such as regenerative fuel cells with hydrogen storage,[2] superconducting magnetic energy storage,[3] lithium ion batteries and supercapacitors,[2b,4] redox flow batteries (RFBs) store energy in the flow liquid electrolyte, decoupling energy density and power density.[5] Even though conventional all-vanadium RFBs with a power/capacity scale up to MW/MWh have been successfully commercialized,[6] the use of toxic and expensive vanadium has limited the widespread application of RFBs. The development of zinc/bromine, zinc/iodide, chromium/iron electrolytes has also been impeded due to their high toxicity and negative environmental impact.[6b,7] Consequently, intense attention has been directed to the investigations of organic redox-active materials with high structural diversity and tunability, low cost, and low toxicity,[5b,c,7f,8] The key factors for electroactive material performance, such as solubility, stability, molecular size, net molecular charge, and redox potential, can be readily tuned by molecular engineering,[5c,9] For example, the incorporation of ammonium unit(s) into the structure improve the solubility in aqueous electrolytes due to their polar nature and shifts the redox potential anodically because of their electron-withdrawing property.[10]

Several classes of organic active materials have been extensively investigated in organic RFBs, including (but not limited to): quinone,[10,11] viologen,[12] 2,2,6,6-tetramethylpiperidine-1-oxyl (TEMPO),[12b,g,13] phenothiazine,[14] and metallocene compounds.[15] Our group has successfully demonstrated the PEGylation (PEG = poly(ethylene glycol)) strategy in organic RFBs using viologen and phenothiazine as the redox active materials.[16] Quinone and its derivatives, such as 2,6-dihydroxyanthraquinone (AQ), are attractive because of their two-electron activity. Progress has been made in anthraquinone-based aqueous RFBs, where a wide range of pH values (1–14) has been employed to fulfil the solubility needs.[11a,b,16] The extremely acidic or basic solvents (such as H_2SO_4 or NaOH) are highly corrosive to the battery device and their use is detrimental to the stability of the redox-active materials. In addition, side reactions of anthraquinones, such as the dimerization and nucleophilic substitution reactions, give rise to irreversible capacity loss,[14,16a,17] resulting in short battery cyclability. While viologen compounds are promising anolytes due to their two-electron activity (two successive one-electron processes), the insufficient solubility of the doubly reduced species (bipyridinylidene) limits the second electron utilization. Although the incorporation of polar groups has improved the solubility of these compounds,[12a,16,18] the crossover of redox materials is still unresolved. TEMPO, phenothiazine, and metallocenes have been successfully applied as catholytes in RFBs, but this approach has several unfavourable features such as tedious synthesis, low stability, and high cost.[14,15,19] For practical applications, an aqueous RFB should possess (1) high electrolyte stability, (2) wide electrochemical window (yet narrower than

[a] Dr. J. Chai,[+] X. Wang,[+] A. Lashgari, C. K. Williams, Prof. J. Jiang
Department of Chemistry
University of Cincinnati
P.O. Box 210172, Cincinnati, Ohio 45221-0172, (USA)
E-mail: jianbing.jiang@uc.edu

[+] These authors contributed equally to this work.

Supporting information for this article is available on the WWW under https://doi.org/10.1002/cssc.202001286

the water splitting window), (3) high electrolyte solubility, and (4) mitigated crossover (Figure 1). Currently, few (if any) aqueous RFB satisfies all four criteria.

Much attention has been focused on molecular engineering strategies for the optimization of electrolyte performance, but here we report a distinct micellization strategy, which enlarges the overall molecular size by forming micelles, to alleviate crossover and parasitic reactions. The RFBs using the micellization strategy demonstrate good cyclability in pH-neutral aqueous electrolyte. PEGylated compounds PEG3-AQ, PEG12-AQ, and PEG45-AQ (PEG*n* denotes *n* ethylene oxide units) were synthesized via one-step synthesis with high purity and high yields. We investigate the ease of synthesis, electrochemical performance of the micellar anthraquinones, battery performance, and parasitic side reaction mechanisms of the electrolytes using organic synthesis, proton nuclear resonance spectroscopy (^{1}H NMR), density functional theory (DFT) calculations, cyclic voltammetry (CV), scanning electron microscope (SEM), and fluorescence spectroscopy. When paired with a well-known potassium ferrocyanide catholyte, the micellar PEG12-AQ aqueous RFB presented a high capacity retention of 90.7% after 3600 charge/discharge cycles (28.3 days), with an average Coulombic efficiency of $>$99.9% and capacity retention of 99.67% per day (99.998% per cycle). The pre- and post-cycling electrolyte solutions were neutral, indicating the non-corrosive feature of the aqueous RFB. The absence of the commonly observed dimerized product in the post-cycling electrolyte, together with a concentration-independent control experiment, confirmed the enhanced stability of the anthraquinone compound due to the micellar structure of the anolyte. This work presents a pathway for using micellization to obtain redox-active materials with enhanced performance, which represents a critical advance for the development of highly stable, long-cycling RFBs for practical applications.

Results and Discussion

Molecular design and synthesis

Different molecular engineering strategies have been reported to increase the solubility of anthraquinones in aqueous solution.[10,12b,16] Anthraquinones with different water-solubilizing groups require aqueous solution with distinct acidity for optimal solubility; acidic units, such as alcohol, phosphonic acid, and carboxylic acid, require alkaline solvents for the deprotonation of the substituents for high water solubility,[11a,c,f,16a] whereas sulfonated anthraquinone requires highly acidic H_2SO_4 solution for high solubility.[16] In a critical breakthrough, the Aziz[20] and Liu[10] groups reported on the anthraquinones with oligomeric ethylene glycols and ammonium-bound sulfonate units, respectively, that increase the solubility of anthraquinone in pH-neutral water. The Schubert group reported a core-corona structure for RFB with additional block copolymers in organic solvents.[21] Here, we envisioned a micellar structure of AQ bearing terminal-capped ethylene glycols for (1) high solubility in pH-neutral aqueous solvent, (2) increased molecular size for mitigated crossover, and (3) enhanced AQ stability against intramolecular dimerization and other nucleophilic aromatic substitution side reactions because of the shielding of the hydrophobic heads by the hydrophilic PEG tails. The three analogous compounds (PEG3-AQ, PEG12-AQ and PEG45-AQ. See Scheme S1 in the Supporting Information) examined here allow structure-function relationship studies for the stability, solubility and crossover properties as a function of the PEG chain length. Finally, the biocompatibility and environmentally friendliness of the non-toxic PEG simplifies the disposal procedure of the post-cycling electrolytes. Taken together, the attractive features of the micellization strategy indicate its great application potential in organic material-based aqueous RFBs. Following established synthetic protocol in our previous reports with slight modification,[16] the three anthraquinone compounds were readily synthesized in high yields (85–91%, Scheme S1). All compounds were characterized by ^{1}H NMR, ^{13}C NMR, and high-resolution mass spectrometry prior to the electrochemical and battery measurements.

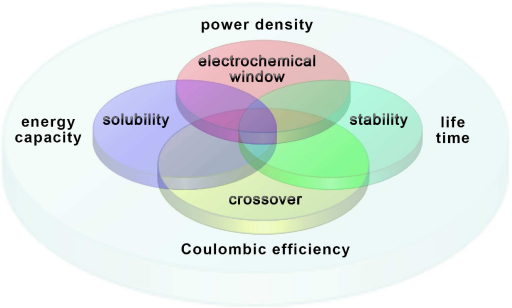

Figure 1. Venn diagram depicting the four key requirements for aqueous RFBs.

Micellization and electrochemical properties

The compound PEG3-AQ has poor solubility in water (less than 10 mM, Figure S1) due to the limited length of its PEG chains, consistent with a previous report.[20] By contrast, PEG12-AQ and PEG45-AQ are completely miscible with water; however, the longer PEG chains of PEG45-AQ led to the high viscosity of the solution, disfavouring its application in RFBs. PEG12-AQ possesses the advantages of both high solubility and low viscosity, and thus is the primary focus of this study.

The formation and size of micelles of the PEGylated anthraquinones were confirmed by Scanning Electron Microscope (SEM) (Figure 2b and Figure S2a). The diameter of the spherical PEG12-AQ micelle was observed as about 44.1 nm (Figure S2b), the obvious Tyndall effect shown in Figure S2c further proves the existence of micelles and colloids. The critical micelle concentration (CMC) was determined to be 0.013 mM (0.016 g/L) in 0.5 M KCl at 25 °C (Figure S3). All of the compounds were subjected to CV measurements in a pH-neutral 0.5 M KCl electrolyte. The redox couple of PEG12-AQ

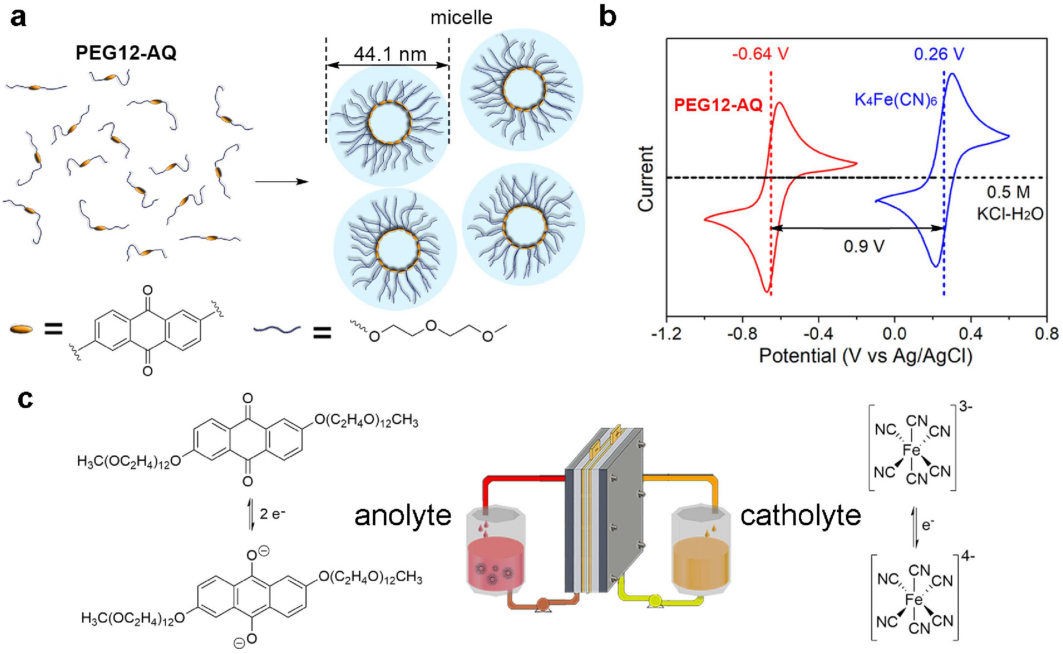

Figure 2. a) Micelle structure of PEG12-AQ with aqueous electrolytes. b) CVs of PEG12-AQ (red) and $K_4Fe(CN)_6$ (blue); conditions: 5 mM of each electrolyte in a 0.5 M KCl aqueous solution, the dotted line is the CV scan of blank 0.5 M KCl electrolyte. All CV measurements were performed at a sweep rate of 50 mV s^{-1}. c) battery reactions of PEG12-AQ and $K_4Fe(CN)_6$.

was fully reversible with a median potential of −0.64 V vs Ag/AgCl (Figure 2c), showing that the PEG groups do not influence redox potential (see Table S1 for the redox potentials of various AQ compounds). The reversible redox events and peak separation (65 mV) indicate that the formation of micelles did not impact the electronic communication between the electrode and shielded anthraquinone arrays. Paired with potassium ferrocyanide, $K_4Fe(CN)_6$, the battery possesses a theoretical potential of 0.9 V. By contrast, compounds PEG3-AQ and PEG45-AQ showed unsatisfactory redox reversibility due to the limited water solubility and/or entanglement of the anthraquinone molecules with the long PEG segments, respectively (Figure S4). To study the effect of the PEG chains on the electrochemical properties of the PEGylated anthraquinone compounds, DFT calculations of AQ and PEG12-AQ in two charge states were carried out to investigate the electron density distributions of AQ and PEG12-AQ. The results show that for both AQ and PEG12-AQ, the highest occupied molecular orbital (HOMO) and lowest unoccupied molecular orbitals (LUMO) are almost the same and mapped through AQ rings symmetrically (Figure S5). The energy gaps (E_g) of the different redox states of AQ and PEG12-AQ are the same, indicating that the presence of the PEG unit does not affect the electrochemical properties. The E_g of the original oxidation state is higher than E_g of the two-electron reduced state for both AQ and PEG12-AQ, showing that a higher energy is required for the electron transfer in redox reactions.

Pourbaix studies on the micellar PEG12-AQ (Figure S6) revealed that the number of protons participating in the redox reaction of PEG12-AQ is nearly pH-independent in a wide pH range (3.5–10.5), indicating the formation of a hydration shell on the PEG chains in close proximity to the anthraquinone cluster that facilitates proton transfer steps during the proton-coupled electron transfer reactions (see more details in Supporting information).[11g,22]

The kinetic properties of the PEG12-AQ micelle solution were studied using rotating disk electrode measurements (Figure 3a). The linear Levich plot of PEG12-AQ (Figure 3b) was established based on the limiting currents and the square root of the angular velocity. The diffusion coefficient is obtained from the Levich equation [Eq. (1) in the Supporting Information][11c,12a] and was determined to be 2.236×10^{-6} $cm^2 s^{-1}$, which was comparable to those of the reported anthraquinones in the pH-neutral electrolyte (see Supporting Information for the calculation of the diffusion coefficients).[10,23] The high diffusion coefficient of micellar species is probably due to the dissociation of micelle into single anthraquinone molecules during the measurement under reductive conditions. Furthermore, to obtain the kinetic rate constant (k_0) and transfer coefficient (α), we fitted the limited currents to the Butler-Volmer equation (Equations 2 and 3 in Supporting Information)[8c,11a,c] and obtained a k_0 of 1.59×10^{-2} $cm\,s^{-1}$ and a α of 0.59 (Figure 3b–d) [see the Supporting Information for the calculations of k_0 and α]. Both values are comparable to or exceed those of the inorganic redox couples employed in aqueous flow batteries.[15a,24] These parameters are in agreement with the corresponding parameters obtained for other anthraquinones in aqueous RFBs,[11c] indicating that the micellization of PEG12-AQ does not sacrifice the promising electrochemical features of these compounds.

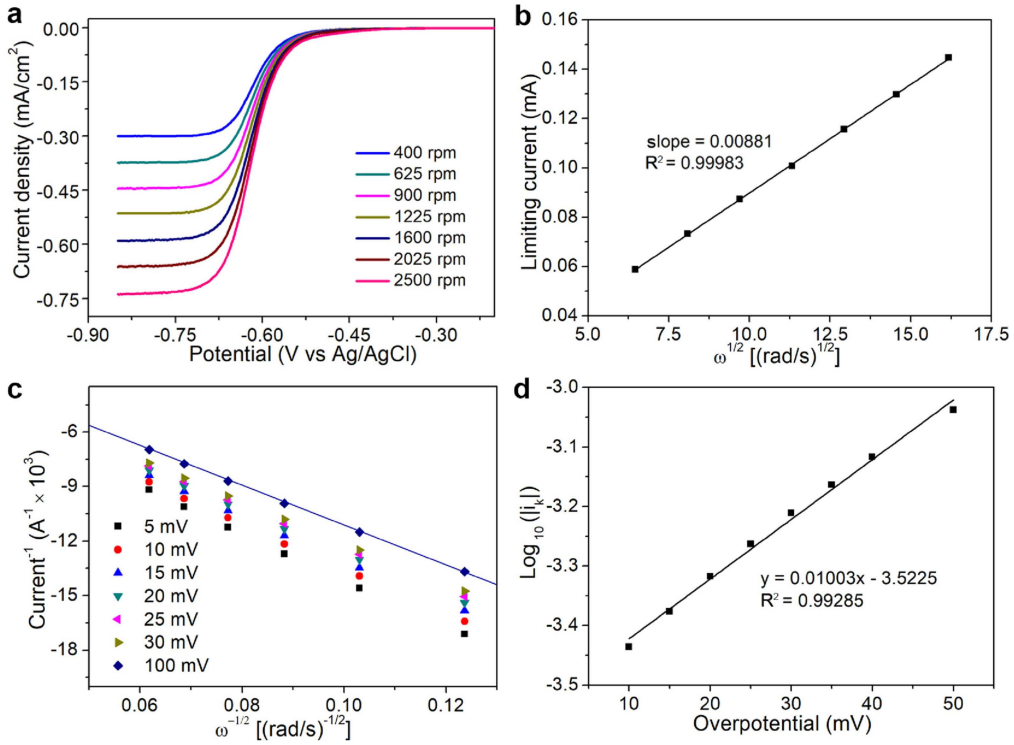

Figure 3. Kinetic properties of PEG12-AQ. a) Linear sweep voltammetry plots obtained at different rotation rates of the rotating disk electrode. b) Peak oxidation and reduction current density at different square roots of angular velocity. c) Koutecký–Levich curve (current^{-1} vs $\omega^{-1/2}$) at different reduction overpotentials. d) Tafel plot constructed using the current response and overpotentials. Solution: 1.0 mM PEG12-AQ in a 0.50 M KCl aqueous solution.

Battery performance characteristics

The full battery test employs 6.5 mL of 100 mM PEG12-AQ and 75 mM $K_4Fe(CN)_6$/25 mM $K_3Fe(CN)_6$ in 50 mL 0.5 M KCl aqueous solution. Excess of mixed $K_4Fe(CN)_6$/$K_3Fe(CN)_6$ catholyte was used to allow complete electrochemical conversion of the anolyte PEG12-AQ. The open-circuit voltage (OCV) increased from 0.847 V at 10% state of charge (SOC) to 1.01 V at 100% SOC (Figure 4a). The high-frequency area specific resistance (ASR) that predominantly reflects the resistance of the separator, contributes approximately 70% of the polarization ASR of the entire battery (Figures 4a and S7). In addition, the polarization curve of the power density and current density (Figures 4b and S8) exhibits the highest current power density of greater than 80 mW cm^{-2}.[25] It should be noted that, although not demonstrated, the power density can be improved by using selective permeable membranes with higher ionic conductivity.[5c,d]

The rate performance of the battery largely reflects its electrochemical stability under fast charge/discharge conditions. The battery was galvanostatically charged/discharged at current densities varying from 20 to 100 mA cm^{-2} (Figure 4c). At each current density, the battery was cycled 10 times. At a low current density of 20 mA cm^{-2}, the battery delivered a discharge capacity of 30.7 mAh, accounting for 88.2% of the theoretical capacity. The battery presented high efficiencies, including a coulombic efficiency (CE) of 99.8%, an energy efficiency (EE) of 87.6%, and a voltage efficiency (VE) of 87.8% (Figure 4d). At a high current density of 100 mA cm^{-2}, the battery still delivered a discharge capacity of 24.6 mAh. The CE, EE, and VE efficiencies were still 99.6%, 48.9%, and 49.1%, respectively. The high performance of the PEG12-AQ-based RFB benefits from the low impedance of the battery and fast kinetics of the electroactive materials in the electrolyte.

Long cyclability is a key parameter for the evaluation of the feasibility of RFBs for practical applications.[26] As found in the rate performance study (Figure 4c), the PEG12-AQ/$K_4Fe(CN)_6$ battery presented a high coulombic efficiency of over 99.9% and a high capacity utilization of 83.8% at 60 mA cm^{-2}. Thus, the battery was galvanostatically charged/discharged at 60 mA cm^{-2} for the long cyclability evaluation. After an activation process of five galvanostatic-potentiostatic charge/discharge cycles (Figure S9), the battery displayed excellent capacity retention (Figure 5a) and stable charge/discharge profiles (Figure 5b). In the first 1200 cycles, the battery had a capacity retention of 99.999% per cycle and a coulombic efficiency of 99.93%. After 1200 cycles, 0.4 mL electrolytes were sampled from the reservoirs for CV and ^{1}H NMR analysis, causing a slight capacity drop (Figure 5a and Figure S10). From 1201st to 2400th cycles, the capacity retention of the battery showed a slight decrease that was related to the gradual increase of the high-frequency impedance (Figure 5c). The increased impedance may originate from a trace amount of the PEG12-AQ deposited on the separator that slightly limits the transport of K^+ through the separator. Nevertheless, the battery still presented a capacity retention of 99.995% per cycle and a

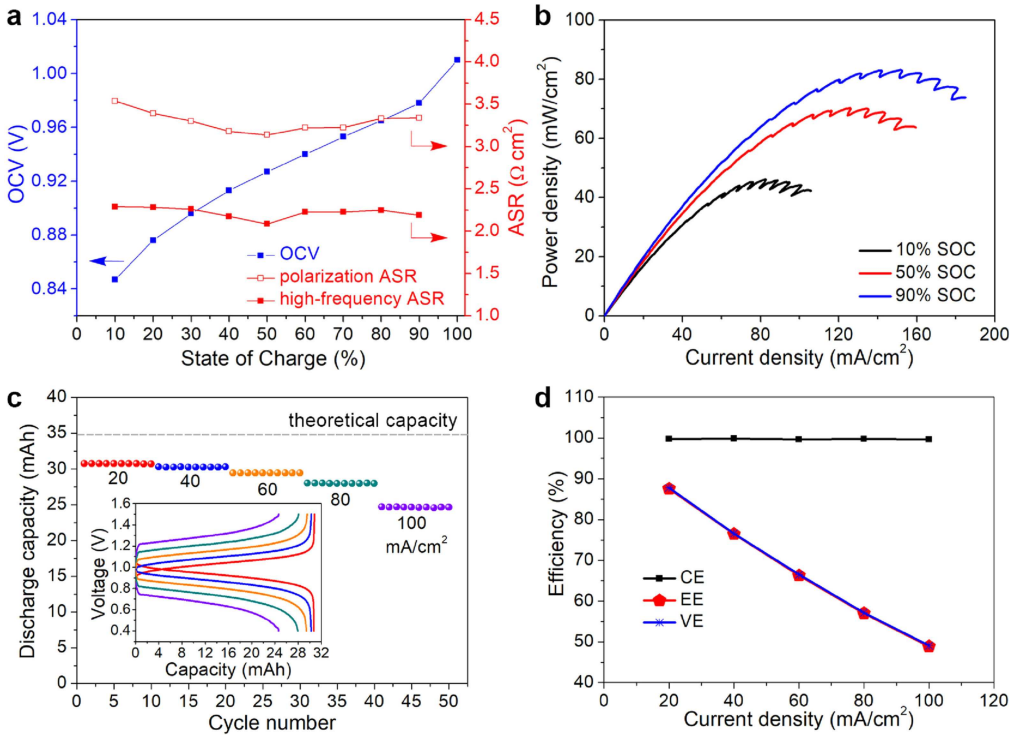

Figure 4. Polarization and rate ability of the 100 mM PEG12-AQ/$K_4Fe(CN)_6$ battery: a)OCV, high-frequency ASR, and polarization ASR of the battery vs the state of charge (SOC). b) Polarizations of the battery at 10%, 50% and 90% SOC. c) Discharge capacity; inset: charge/discharge profiles. d) Coulombic efficiency (CE), energy efficiency (EE), and voltage efficiency (VE) at current densities from 20 to 100 mA cm^{-2}.

Coulombic efficiency of 99.9%. The same amount of anolyte solution (0.4 mL) was sampled after the 2400th cycle for mechanistic analysis. The cycling performance for the last 1200 cycles (from 2401st to 3600th cycles) is almost identical to that for the middle 1200 cycles, indicative of the high and steady cycling stability of the battery. The overall capacity retention is 90.7% with an average Coulombic efficiency of 99.9% for all 3600 cycles (28.3 days), and the average capacity retention is 99.998% per cycle and 99.67% per day. Please note that all calculations are based on the original volume of the anolyte disregarding the volume changes due to two electrolyte samplings carried out for mechanistic studies (0.4 mL for each sampling) (Figure S10). To the best of our knowledge, this work represents the longest consecutive running time and the highest charge/discharge cycles among the reported organic material-based aqueous RFBs.

Mechanistic analysis of post-cycling electrolytes

It has been widely reported that during charge/discharge processes, AQs are susceptible to side reactions such as anthrone formation, dimerization, and nucleophilic reactions (Figure S11),[14,16a,17] that are the main causes of the irreversible capacity loss for anthraquinone-based RFBs. To confirm whether any of these side reactions occurred during the charge/discharge process, the post-cycling anolyte and post-cycling catholyte solutions were analysed using CV and ^{1}H NMR spectroscopy. No additional redox peak was observed in CV (Figure 5d), and no PEG12-AQ or $K_4Fe(CN)_6$ redox peak was observed in their counter reservoirs (Figure 5d), indicating suppressed crossover. It should be noted that sampling during cycling contributes to the current decrease of the CV curve (Figure 5d). As a cation exchanging membrane, the Fumasep separator effectively inhibits the crossover of $Fe(CN)_6^{4-}$ via the Donnan exclusion mechanism.[27] For the charge-neutral PEG12-AQ and the negatively charged $(PEG12\text{-}AQ)^{2-}$, the crossover is suppressed via the size-exclusion mechanism due to the enlarged molecular size resulting from the micellization. The ^{1}H NMR spectra of the PEG12-AQ anolyte before cycling, and after 1200, 2400, and 3600 cycles were also recorded (Figure S12), and no new peaks were observed, suggesting the high stability of the PEG12-AQ anolyte. The pH of the post-cycling anolyte and catholyte are neutral, indicating that the battery is non-corrosive. The diameter of the micelles after 3600 cycles increased to 55.2 nm (Figure S13), presumably due to the charge-induced polarity change that in turn led to micelle dissociation and reconstruction.[21] During charging, the number of micelles decreases as a result of increase hydrophilicity on the AQ molecules. During the discharging process, as the PEG12-AQ anions lose electrons, the anthraquinone molecules become amphiphilic molecules again, and the reconstruction of the micelles dominates. In the whole dynamic micellar dissociation-reconstruction process, the number of micelles varies with discharge and charge continuously. It is not surprising that size of micelle is changing, and the size of micelle obviously more

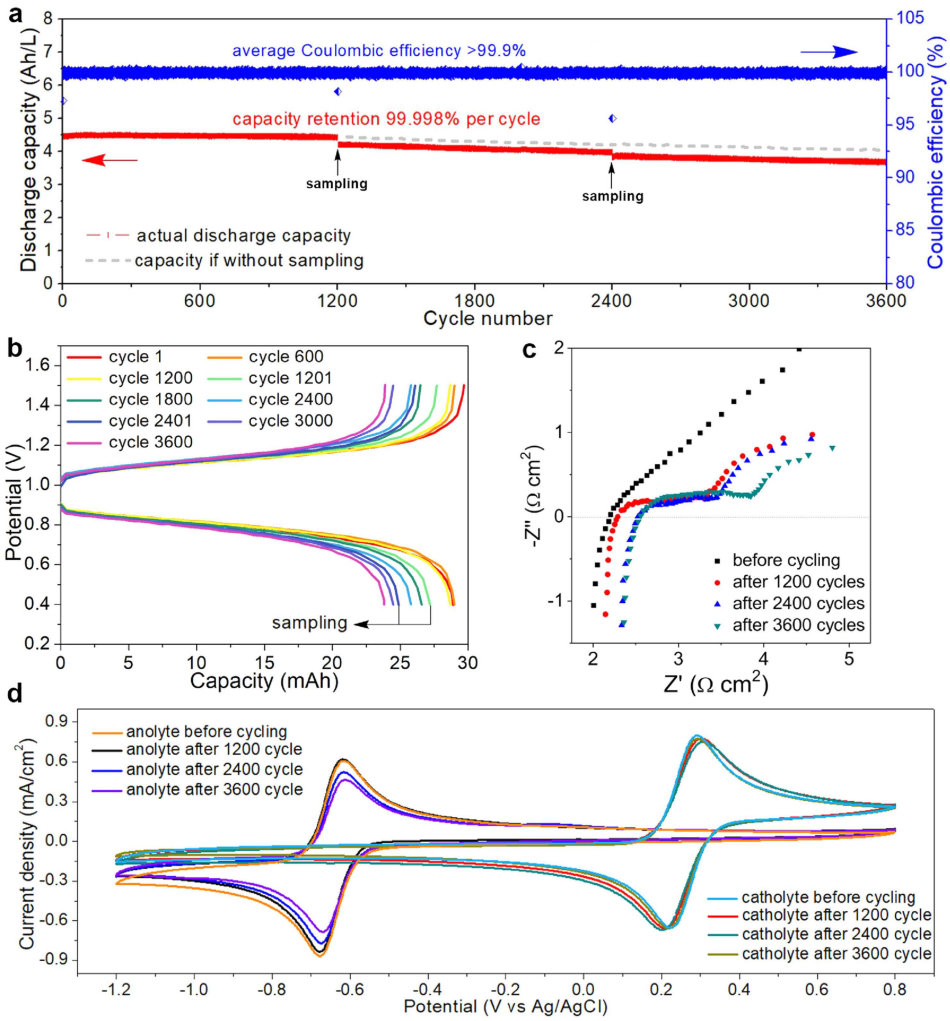

Figure 5. Long cycling properties of the 100 mM PEG12-AQ-based battery. a) Discharge capacity, coulombic efficiency over 3600 cycles at 60 mA cm^{-2}. b) Charge/discharge profiles at different cycle numbers. c) Electrochemical impedance spectroscopy before cycling and after 1200, 2400, and 3600 cycles. d) CV scans of anolyte and catholyte before cycling and after 1200, 2400, and 3600 cycles. The electrolytes were diluted to one fifth for CV measurements.

conducive to suppress the crossover and maintain superb battery cyclability.

The rate of dimer formation via intermolecular dimerization increases with increased concentration. To verify the absence of the intramolecular dimerization reaction during the charge/discharge process, the same PEG12-AQ/$K_4Fe(CN)_6$ battery was assembled and tested at the same conditions except for the lower concentration of the electrolytes (25 mM PEG12-AQ in 0.5 M KCl aqueous solution) (Figures S14–16). This battery displayed equally excellent capacity retention and high coulombic efficiency over 1200 cycles (Figure S14), indicating that the concentration of PEG12-AQ had no negative effect on the battery performance, thus demonstrating the absence of the dimerization reaction during the charge/discharge process. It is concluded that PEG12-AQ is different from other anthraquinone molecules with respect to the susceptibility to parasitic reactions. The excellent performance of PEG12-AQ is most likely due to protection of the anthraquinone framework by the hydrodynamic PEG chains that prevents the intermolecular dimerization reaction and nucleophilic attack from the nucleophiles such as water molecules in the medium.

Higher concentration battery

The battery performance using concentrated electrolytes is critical when evaluating the potential of RFBs. A 0.35 M PEG12-AQ/KCl micellization solution (0.7 M electron concentration) is investigated as anolyte to demonstrate the feasibility using higher PEG12-AQ concentration. The discharge capacity, Coulombic efficiency, and charge/discharge profiles of the battery are presented in Figure 6a and 6b. The battery presented a high Coulombic efficiency of 99.9% and a capacity retention of 99.98% per cycle at 60 mA cm^{-2} for 180 cycles, which is also attributed to the high stability of the PEG12-AQ and micellization strategy. In addition, the highest current power density of this battery increases to 120 mW cm^{-2} (Figure 6c) owing to increased electrolyte concentration, the theoretical energy

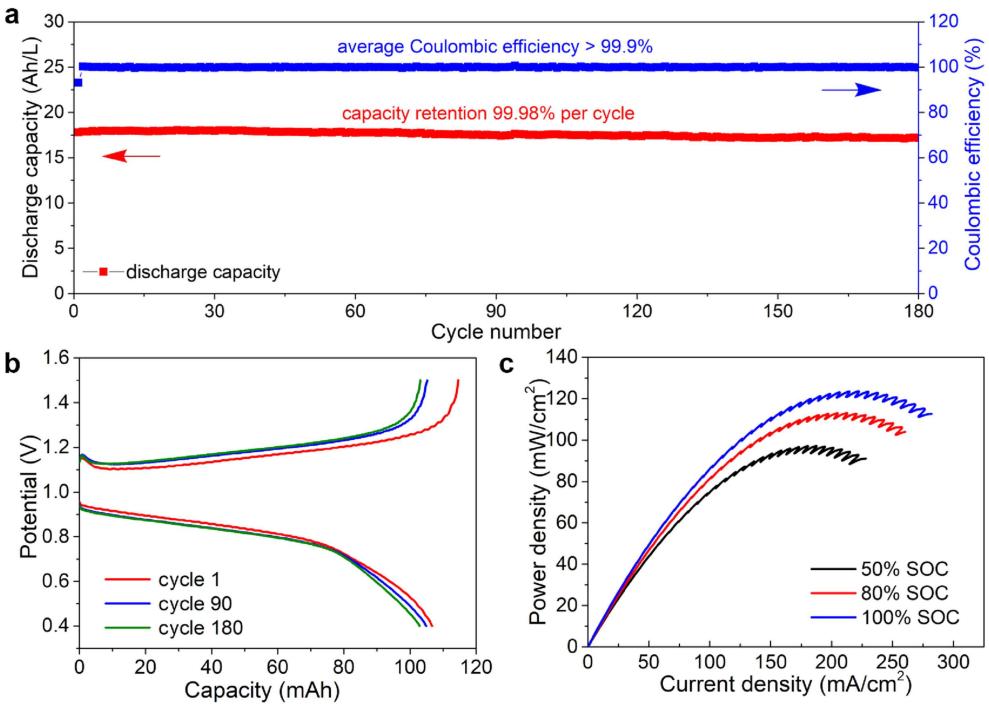

Figure 6. Performances of the 350 mM PEG12-AQ-based battery. a) Discharge capacity and coulombic efficiency of the PEG12-AQ (0.35 M)/$K_4Fe(CN)_6$ battery over 180 cycles at 60 mA cm^{-2}. b) Charge/discharge profiles at different cycle numbers. c) Polarizations of the battery at 50%, 80%, and 100% SOC.

density reaches 1.8 Wh L^{-1} (see the Supporting Information for calculation details). Even higher concentration of PEG12-AQ (0.5 M, equivalent to 1.0 M electron concentration) in battery was attempted; however, the cycling was impeded by the high viscosity of the resultant PEG12-AQ electrolyte solution.

Conclusions

We report a micellization strategy based on amphiphilic organic materials and demonstrate long cyclability of an aqueous redox-flow battery (RFB) using a non-toxic, metal-free, and non-corrosive poly(ethylene glycol) (PEG)-modified anthraquinone (AQ) anolyte. The micellization of the PEGylated material enhanced the water solubility, stability, and molecular size to suppress crossover. The PEG12-AQ/$K_4Fe(CN)_6$ battery delivered an excellent cycling performance for over 3600 cycles with an average coulombic efficiency above 99.9% and capacity retention of 99.998% per cycle. Mechanistic analysis was carried out to investigate the possible side reactions and validate the high stability of the anolyte originating from the micellization. The micellization strategy was shown to be effective for overcoming the issues of solubility and stability of organic compounds and provides a promising strategy for the development of pH-neutral aqueous RFBs for practical applications.

Experimental Section

Chemicals and manipulations. All chemicals were purchased from Sigma-Aldrich, stored in an argon-filled glovebox and used as received. The NMR analysis was performed at room temperature using a Bruker AV 400 MHz spectrometer. The unit of chemical shifts is based on ppm. ESI–MS analysis was performed on an Orbitrap Fusion Lumos mass spectrometer from Thermo Scientific. The fluorescence spectra were recorded on a Cary Eclipse fluorescence spectrophotometer. Reported procedures with modifications were followed to prepare the three anthraquinone compounds.[16]

Synthesis of PEG3-AQ. A sample of PEG3-OTs (1.1 g, 3.3 mmol, 2.2 eq), was added to the solution of 2,6-dihydroxyanthraquinone (0.36 g, 1.5 mmol, 1.0 eq) and potassium carbonate (0.83 g, 6.0 mmol, 4.0 eq) in DMF (10 mL). The mixture was stirred under argon at 120 °C for 24 h. After removing DMF under vacuum, the solution was washed with brine and extracted with CH_2Cl_2. The organic extract was combined and dried over Na_2SO_4. The solution was filtered, and the filtrate was dried via rotavape. The crude residue was purified by column chromatography (SiO_2; 5–10% methanol in CH_2Cl_2) to afford the title compound as a yellow powder. Yield: 0.73 g, 91%. ^{1}H NMR (400 MHz, $CDCl_3$): $\delta = 3.41$ (s, 6H), 3.54–3.60 (m, 4H), 3.66–3.75 (m, 8H), 3.76–3.81 (m, 4H), 3.89–4.01 (m, 4H), 4.28–4.38 (m, 4H), 7.28–7.32 (m, 2H), 7.71–7.74 (d, $J =$ 4.0 Hz, 2H), 8.21–8.26 ppm (d, $J = 8.0$ Hz, 2H); ^{13}C NMR (100 MHz, $CDCl_3$): $\delta = 58.91$, 67.98, 69.29, 70.47, 70.54, 70.80, 71.81, 110.46, 120.85, 126.98, 129.48, 135.52, 163.51, 181.86 ppm; HR-MS obsd 533.2383, calcd 533.2381 ($[M+H]^+$, $M = C_{28}H_{36}O_{10}$).

Synthesis of PEG12-AQ. A sample of PEG12-OTs (3.6 g, 5.1 mmol, 2.2 eq) and potassium carbonate (1.3 g, 9.2 mmol, 4.0 eq) were added to the solution of 2,6-dihydroxyanthraquinone (0.72 g, 2.3 mmol, 1.0 eq) in DMF (20 mL) and stirred under argon for 24 h at 120 °C. The solution was washed with brine and extracted with

ethyl acetate. The organic extract was combined and dried over Na_2SO_4. The solution was filtered, and the filtrate was dried via rotavap. The crude residue was purified by column chromatography (SiO_2; 5–10% MeOH in CH_2Cl_2) to afford the title compound as a yellow oil. Yield: 3.68 g, 93%. ^{1}H NMR (400 MHz, $CDCl_3$): $\delta = 3.37$ (s, 6H), 3.40–3.87 (m, 88H), 3.87–3.96 (m, 4H), 4.25–4.38 (m, 4H), 7.26–7.29 (m, 2H), 7.65–7.76 (d, $J = 4$ Hz, 2H), 8.16–8.28 ppm (d, $J = 8$ Hz, 2H); ^{13}C NMR (100 MHz, $CDCl_3$): $\delta = 58.87$, 67.99, 69.27, 70.31–70.53 (m), 70.76, 71.77, 110.46, 120.84, 126.97, 129.49, 135.52, 163.43, 181.64 ppm; HR-MS obsd 1347.6917, calcd 1347.6919 ($[M+Na]^+$, $M = C_{64}H_{108}O_{28}$).

Synthesis of PEG45-AQ. A sample of PEG45-OTs (3.2 g, 1.5 mmol, 3.0 eq) was added to the solution of 2,6-dihydroxyanthraquinone (0.12 g, 0.5 mmol, 1.0 eq) and potassium carbonate (0.28 g, 2.0 mmol, 4.0 eq) in DMF (3.5 mL). The mixture was stirred under argon at 120 °C for 24 h. After removing DMF under vacuum, the solution was washed with brine and extracted with CH_2Cl_2. The organic extract was combined and dried over Na_2SO_4. The solution was filtered, and the filtrate was dried via rotavap. The crude residue was purified by column chromatography (SiO_2; 5–10% methanol in CH_2Cl_2) to afford the title compound as a light-yellow powder. Yield: 1.8 g, 85%. ^{1}H NMR (400 MHz, $CDCl_3$): $\delta = 3.38$ (s, 6H), 3.44–3.72 (m, 344H), 3.73–3.77 (m, 4H), 3.78–3.85 (t, $J = 4.0$ Hz, 4H), 3.88–3.96 (t, $J = 4.0$ Hz, 4H), 4.29–4.34 (t, $J = 4.0$ Hz, 4H), 7.27–7.31 (m, 2H), 7.71–7.74 (d, $J = 4.0$ Hz, 2H), 819–8.26 ppm (d, $J = 8.0$ Hz, 2H); ^{13}C NMR (100 MHz, $CDCl_3$): $\delta = 58.99$, 61.60, 62.22, 68.06, 69.31, 69.66–71.23 (m), 71.84, 72.46, 110.53, 121.02, 127.12, 129.62, 135.65, 163.59, 181.98 ppm; HR-MS obsd 1431.7973, calcd 1431.7997 ($[M+Na+H+K]^{3+}$, $M = C_{196}H_{372}O_{94}$).

SEM measurements. The tests were performed using a JEOL JSM-7500F in SEM mode. A 10 mM PEG12-AQ aqueous solution was chemically dried using 2.5% glutaraldehyde solution, deionized water, ethanol solutions, and ethanol. The dried sample was mounted on an aluminium stub using double sided carbon tape before it was sputter coated with gold to improve imaging.

CMC measurements. The CMC of PEG12-AQ in 0.5 M KCl aqueous electrolytes was obtained by Cary Eclipse Fluorescence Spectrophotometer using pyrene as the fluorescent probe, as previously described.[28] Firstly, 50 μL of 2.4×10^{-3} M pyrene–acetone solution was added in 50 mL of 0.5 M KCl aqueous solution. The PEG12-AQ was dispersed in 0.5 M KCl solution with concentration ranges from 0.2 to 2×10^{-6} g L^{-1}. Then, the two solutions were mixed at a volume ratio of 1:1 and kept in dark for 12 h. The series of mixed solution were excited at 270 nm, and the emission spectra were recorded in the range of 350–500 nm. The intensity ratios of the excitation peaks at 372 (I_1) and 382 (I_3) nm were calculated and then plotted as a function of logarithm of the PEG12-AQ concentration. The CMC value was determined as the point of intersection of two tangents to the curves of high and low concentrations.

Cyclic voltammetry. Glassy carbon with a diameter of 3 mm was used as the working electrode and was polished with 50 nm Al_2O_3 prior to measurements. Platinum wire (0.5 mm) and Ag/AgCl electrodes were used as the counter and reference electrodes, respectively. A sample of 5 mM PEG12-AQ in 0.5 M KCl solution was degassed with argon before test. All CV data were collected with a Bio-Logic potentiostat at a scan rate of 50 mV/s. In CV measurements at varied pH, the concentrated solutions of KOH and HCl were used to adjust the pH as measured by a pH meter. All CV were collected using concentration of 5 mM.

Battery measurements. RFBs were composed of aluminium alloy plate, polytetrafluoroethylene plate, copper plate, graphite current collector, polytetrafluoroethylene frame and graphite felt electrodes with an active area of 5 cm^2 or 28 cm^2. Fumasep E-620(K) cation exchanged membrane was sandwiched between the two graphite felts because of the lower swelling deformation. All the battery measurements were conducted on a Bio-Logic potentiostat or a Land battery test system. For the 25 mM PEG12-AQ/$K_4Fe(CN)_6$ RFB, 20 mL of 25 mM PEG12-AQ in 0.5 M KCl-H_2O was used as the anolyte and 20 mL of 75 mM $K_4Fe(CN)_6 + 25$ mM $K_3Fe(CN)_6$ in 0.5 M KCl-H_2O as the catholyte, respectively. For the 100 mM PEG12-AQ/$K_4Fe(CN)_6$ RFB, 6.5 mL of 100 mM PEG12-AQ in 0.5 M KCl-H_2O and 50 mL of 75 mM $K_4Fe(CN)_6 + 25$ mM $K_3Fe(CN)_6$ in 0.5 M KCl-H_2O was used as anolyte and catholyte, respectively. For the 0.35 M PEG12-AQ/$K_4Fe(CN)_6$, 6 mL of 0.35 M PEG12-AQ in 0.5 M KCl-H_2O and 50 mL of 225 mM $K_4Fe(CN)_6 + 75$ mM $K_3Fe(CN)_6$ in 0.5 M KCl-H_2O was used as anolyte and catholyte, respectively. The rate performance of battery was tested under various current densities. In the first 5 cycles of the long-cycling study, the battery was tested under galvanostatic and potentiostatic charging/discharging conditions. Then, the battery was galvanostatically charged/discharged in the voltage range of 1.5–0.4 V at a current density of 60 mA cm^{-2}. The impedance of the battery was conducted via electrochemical impedance spectroscopy with a frequency ranging from 200 to 100 mHz. The ^{1}H NMR analysis of the post-cycling anolyte was performed by diluting the electrolyte with D_2O to 20 mM in a J Young NMR tube. The spectra were recorded on a Bruker AV 400 MHz spectrometer.

Computation. All calculations were carried out by using Gaussian 09 software for the original and two-electron reduced states.[29] All oxidation states were optimized at ground states with DFT using B3LYP/6-311 + G(d,p) as the basis sets. The polarizable continuum model (PCM) was selected to optimize all geometries in water to include the solvation effect to the free energies. The molecular orbitals (MOs) and molar volume calculations were carried out with DFT method at B3LYP/6-311 + G(d,p) level. The original ref 29 is now deleted, and the original ref 30 now becomes ref 29. All have been corrected in the reference section.

Acknowledgements

The authors acknowledge the University of Cincinnati for startup funding support, and Ohio Supercomputer Center for providing the computational resources. NMR experiments were performed on a Bruker AVANCE NEO 400 MHz NMR spectrometer funded by NSF-MRI grant CHE-1726092.

Conflict of Interest

The authors declare no conflict of interest.

Keywords: anthraquinone · micelles · neutral electrolytes · poly (ethylene glycol) · redox flow batteries

[1] Z. Shao, Z. Wang, Z. Li, Y. Fan, H. Meng, R. Liu, Y. Wang, A. Hagfeldt, G. Cui, S. Pang, *Angew. Chem. Int. Ed.* **2019**, *58*, 5587; *Angew. Chem.* **2019**, *131*, 5643.
[2] a) M. Winter, R. J. Brodd, *Chem. Rev.* **2004**, *104*, 4245; b) Y. Jin, K. Liu, J. Lang, D. Zhuo, Z. Huang, C. A. Wang, H. Wu, Y. Cui, *Nat. Energy* **2018**, *3*, 732.
[3] a) D. Larcher, J. M. Tarascon, *Nat. Chem.* **2015**, *7*, 19; b) A. S. Arico, P. Bruce, B. Scrosati, J. M. Tarascon, W. Van Schalkwijk, *Nat. Mater.* **2005**, *4*,

366; c) M. Armand, F. Endres, D. R. MacFarlane, H. Ohno, B. Scrosati, *Nat. Mater.* **2009**, *8*, 621; d) Y. Yang, D. Kim, M. Yang, P. Schmuki, *Chem. Commun.* **2011**, *47*, 7746.

[4] a) W. Smith, *J. Power Sources* **2000**, *86*, 74; b) W. Buckles, W. V. Hassenzahl, *IEEE Power Eng. Rev.* **2000**, *20*, 16; c) G. L. Soloveichik, *Chem. Rev.* **2015**, *115*, 11533; d) Q. Zhou, J. Ma, S. Dong, X. Li, G. Cui, *Adv. Mater.* **2019**, *31*, 1902029; e) H. Wang, Y. Liang, T. Mirfakhrai, Z. Chen, H. S. Casalongue, H. Dai, *Nano Res.* **2011**, *4*, 729; f) G. Xu, X. Shangguan, S. Dong, X. Zhou, G. Cui, *Angew. Chem. Int. Ed.* **2020**, *59*, 3400; *Angew. Chem.* **2020**, *132*, 3426.

[5] a) S. O. Tung, S. L. Fisher, N. A. Kotov, L. T. Thompson, *Nat. Commun.* **2018**, *9*, 4193; b) T. Ma, Z. Pan, L. Miao, C. Chen, M. Han, Z. Shang, J. Chen, *Angew. Chem. Int. Ed.* **2018**, *57*, 3158; *Angew. Chem.* **2018**, *130*, 3212; c) Y. Ding, C. Zhang, L. Zhang, Y. Zhou, G. Yu, *Chem. Soc. Rev.* **2018**, *47*, 69; d) J. Winsberg, T. Hagemann, T. Janoschka, M. D. Hager, U. S. Schubert, *Angew. Chem. Int. Ed.* **2017**, *56*, 686; *Angew. Chem.* **2017**, *129*, 702; e) R. F. Service, *Science* **2018**, *362*, 508; f) X. Wei, W. Xu, J. Huang, L. Zhang, E. Walter, C. Lawrence, M. Vijayakumar, W. A. Henderson, T. Liu, L. Cosimbescu, B. Li, V. Sprenkle, W. Wang, *Angew. Chem. Int. Ed.* **2015**, *54*, 8684; *Angew. Chem.* **2015**, *127*, 8808; g) X. Wei, G.-G. Xia, B. Kirby, E. Thomsen, B. Li, Z. Nie, G. G. Graff, J. Liu, V. Sprenkle, W. Wang, *J. Electrochem. Soc.* **2015**, *163*, A5150; h) J. Huang, W. Duan, J. Zhang, I. A. Shkrob, R. S. Assary, B. Pan, C. Liao, Z. Zhang, X. Wei, L. Zhang, *J. Mater. Chem. A* **2018**, *6*, 6251.

[6] a) X. Li, H. Zhang, Z. Mai, H. Zhang, I. Vankelecom, *Energy Environ. Sci.* **2011**, *4*, 1147; b) Y. K. Zeng, T. S. Zhao, L. An, X. L. Zhou, L. Wei, *J. Power Sources* **2015**, *300*, 438.

[7] a) B. Li, J. Liu, Z. Nie, W. Wang, D. Reed, J. Liu, P. McGrail, V. Sprenkle, *Nano Lett.* **2016**, *16*, 4335; b) K. Gong, X. Ma, K. M. Conforti, K. J. Kuttler, J. B. Grunewald, K. L. Yeager, M. Z. Bazant, S. Gu, Y. Yan, *Energy Environ. Sci.* **2015**, *8*, 2941; c) H. Pan, Y. Shao, P. Yan, Y. Cheng, K. S. Han, Z. Nie, C. Wang, J. Yang, X. Li, P. Bhattacharya, *Nat. Energy* **2016**, *1*, 16039; d) D. Kundu, B. D. Adams, V. Duffort, S. H. Vajargah, L. F. Nazar, *Nat. Energy* **2016**, *1*, 16119; e) H. Wang, H. Dai, *Chem. Soc. Rev.* **2013**, *42*, 3088; f) X. Wei, W. Pan, W. Duan, A. Hollas, Z. Yang, B. Li, Z. Nie, J. Liu, D. Reed, W. Wang, V. Sprenkle, *ACS Energy Lett.* **2017**, *2*, 2187.

[8] a) C. Zhang, Z. Niu, Y. Ding, L. Zhang, Y. Zhou, X. Guo, X. Zhang, Y. Zhao, G. Yu, *Chem* **2018**, *4*, 2814; b) C. Zhang, L. Zhang, Y. Ding, X. Guo, G. Yu, *ACS Energy Lett.* **2018**, *3*, 2875; c) K. Lin, R. Gómez Bombarelli, E. S. Beh, L. Tong, Q. Chen, A. Valle, A. Aspuru-Guzik, M. J. Aziz, R. G. Gordon, *Nat. Energy* **2016**, *1*, 16102; d) T. Janoschka, N. Martin, U. Martin, C. Friebe, S. Morgenstern, H. Hiller, M. D. Hager, U. S. Schubert, *Nature* **2015**, *527*, 78; e) S. E. Doris, A. L. Ward, A. Baskin, P. D. Frischmann, N. Gavvalapalli, E. Chénard, C. S. Sevov, D. Prendergast, J. S. Moore, B. A. Helms, *Angew. Chem. Int. Ed.* **2017**, *56*, 1595; *Angew. Chem.* **2017**, *129*, 1617; f) J. Luo, B. Hu, M. Hu, Y. Zhao, T. L. Liu, *ACS Energy Lett.* **2019**, *4*, 2220; g) P. Navalpotro, J. Palma, M. Anderson, R. Marcilla, *Angew. Chem. Int. Ed.* **2017**, *56*, 12460; *Angew. Chem.* **2017**, *129*, 12634; h) X. Wei, W. Duan, J. Huang, L. Zhang, B. Li, D. Reed, W. Xu, V. Sprenkle, W. Wang, *ACS Energy Lett.* **2016**, *1*, 705.

[9] a) G. Nagarjuna, J. Hui, K. J. Cheng, T. Lichtenstein, M. Shen, J. S. Moore, J. Rodriguez-Lopez, *J. Am. Chem. Soc.* **2014**, *136*, 16309; b) N. Gallagher, H. Z. Ye, J. Lopez, Y. Zhu, T. Van Voorhis, Y. Shao-Horn, J. A. Johnson, *Angew. Chem. Int. Ed.* **2020**, *59*, 3952; *Angew. Chem.* **2020**, *132*, 3980.

[10] B. Hu, J. Luo, M. Hu, B. Yuan, T. L. Liu, *Angew. Chem. Int. Ed.* **2019**, *58*, 16629; *Angew. Chem.* **2019**, *131*, 16782.

[11] a) K. Lin, Q. Chen, M. R. Gerhardt, L. Tong, S. B. Kim, L. Eisenach, A. W. Valle, D. Hardee, R. G. Gordon, M. J. Aziz, *Science* **2015**, *349*, 1529; b) Y. Ding, Y. Li, G. Yu, *Chem* **2016**, *1*, 790; c) B. Huskinson, M. P. Marshak, C. Suh, S. Er, M. R. Gerhardt, C. J. Galvin, X. Chen, A. Aspuru-Guzik, R. G. Gordon, M. J. Aziz, *Nature* **2014**, *505*, 195; d) L. Tong, Y. Jing, R. G. Gordon, M. J. Aziz, *ACS Appl. Energy Mater.* **2019**, *2*, 4016; e) Z. J. Yang, L. C. Tong, D. P. Tabor, E. S. Beh, M. A. Goulet, D. De Porcellinis, A. Aspuru-Guzik, R. G. Gordon, M. J. Aziz, *Adv. Energy Mater.* **2018**, *8*, 1702056; f) D. G. Kwabi, K. Lin, Y. Ji, E. F. Kerr, M.-A. Goulet, D. De Porcellinis, D. P. Tabor, D. A. Pollack, A. Aspuru Guzik, R. G. Gordon, M. J. Aziz, *Joule* **2018**, *2*, 1894; g) M. Quan, D. Sanchez, M. F. Wasylkiw, D. K. Smith, *J. Am. Chem. Soc.* **2007**, *129*, 12847.

[12] a) C. DeBruler, B. Hu, J. Moss, X. Liu, J. Luo, Y. Sun, T. L. Liu, *Chem* **2017**, *3*, 961; b) Y. Liu, M.-A. Goulet, L. Tong, Y. Liu, Y. Ji, L. Wu, R. G. Gordon, M. J. Aziz, Z. Yang, T. Xu, *Chem* **2019**, *5*, 1861; c) E. S. Beh, D. De Porcellinis, R. L. Gracia, K. T. Xia, R. G. Gordon, M. J. Aziz, *ACS Energy Lett.* **2017**, *2*, 639; d) J. Luo, W. Wu, C. Debruler, B. Hu, M. Hu, T. L. Liu, *J. Mater. Chem. A* **2019**, *7*, 9130; e) E. C. Montoto, G. Nagarjuna, J. S. Moore, J. Rodríguez-López, *J. Electrochem. Soc.* **2017**, *164*, A1688; f) M. Burgess, E. Chénard, K. Hernández-Burgos, G. Nagarjuna, R. S. Assary, J. Hui, J. S. Moore, J. Rodríguez-López, *Chem. Mater.* **2016**, *28*, 7362; g) T. Janoschka, N. Martin, M. D. Hager, U. S. Schubert, *Angew. Chem. Int. Ed.* **2016**, *55*, 14427; *Angew. Chem.* **2016**, *128*, 14639.

[13] a) X. Wei, W. Xu, M. Vijayakumar, L. Cosimbescu, T. Liu, V. Sprenkle, W. Wang, *Adv. Mater.* **2014**, *26*, 7649; b) J. Winsberg, T. Janoschka, S. Morgenstern, T. Hagemann, S. Muench, G. Hauffman, J. F. Gohy, M. D. Hager, U. S. Schubert, *Adv. Mater.* **2016**, *28*, 2238; c) T. Liu, X. Wei, Z. Nie, V. Sprenkle, W. Wang, *Adv. Energy Mater.* **2016**, *6*, 1501449.

[14] C. Zhang, Z. Niu, S. Peng, Y. Ding, L. Zhang, X. Guo, Y. Zhao, G. Yu, *Adv. Mater.* **2019**, *31*, e1901052.

[15] a) Y. Ding, Y. Zhao, Y. Li, J. B. Goodenough, G. Yu, *Energy Environ. Sci.* **2017**, 10, 491; b) B. Hwang, M. S. Park, K. Kim, *ChemSusChem* **2015**, *8*, 310.

[16] a) J. Chai, A. Lashgari, Z. Cao, C. K. Williams, X. Wang, J. Dong, J. J. Jiang, *ACS Appl. Mater. Interfaces* **2020**, *12*, 15262; b) J. Chai, A. Lashgari, X. Wang, C. K. Williams, J. J. Jiang, *J. Mater. Chem. A* **2020**, DOI: 10.1039/d0ta02303e.

[17] a) Y. Ji, M. A. Goulet, D. A. Pollack, D. G. Kwabi, S. Jin, D. Porcellinis, E. F. Kerr, R. G. Gordon, M. J. Aziz, *Adv. Energy Mater.* **2019**, *9*, 1900039; b) W. Wang, W. Xu, L. Cosimbescu, D. Choi, L. Li, Z. Yang, *Chem. Commun.* **2012**, *48*, 6669; c) M. R. Gerhardt, L. Tong, R. Gómez Bombarelli, Q. Chen, M. P. Marshak, C. J. Galvin, A. Aspuru-Guzik, R. G. Gordon, M. J. Aziz, *Adv. Energy Mater.* **2017**, *7*, 1601488.

[18] a) A. Hollas, X. Wei, V. Murugesan, Z. Nie, B. Li, D. Reed, J. Liu, V. Sprenkle, W. Wang, *Nat. Energy* **2018**, *3*, 508; b) M. A. Goulet, L. Tong, D. A. Pollack, D. P. Tabor, S. A. Odom, A. Aspuru-Guzik, E. E. Kwan, R. G. Gordon, M. J. Aziz, *J. Am. Chem. Soc.* **2019**, *141*, 8014.

[19] a) B. Hu, T. L. Liu, *J. Energy Chem.* **2018**, 27, 1326; b) B. Hu, Y. Tang, J. Luo, G. Grove, Y. Guo, T. L. Liu, *Chem. Commun.* **2018**, *54*, 6871.

[20] S. Jin, Y. Jing, D. G. Kwabi, Y. Ji, L. Tong, D. De Porcellinis, M.-A. Goulet, D. A. Pollack, R. G. Gordon, M. J. Aziz, *ACS Energy Lett.* **2019**, *4*, 1342.

[21] T. Hagemann, M. Strumpf, E. Schröter, C. Stolze, M. Grube, I. Nischang, M. D. Hager, U. S. Schubert, *Chem. Mater.* **2019**, *31*, 7987.

[22] J. Winsberg, S. Muench, T. Hagemann, S. Morgenstern, T. Janoschka, M. Billing, F. H. Schacher, G. Hauffman, J.-F. Gohy, S. Hoeppener, M. D. Hager, U. S. Schubert, *Polym. Chem.* **2016**, *7*, 1711.

[23] M. A. B. H. Susan, M. Begum, Y. Takeoka, M. Watanabe, *J. Electroanal. Chem.* **2000**, *481*, 192.

[24] R. S. Nicholson, *Anal. Chem.* **1965**, *37*, 1351.

[25] A. Z. Weber, M. M. Mench, J. P. Meyers, P. N. Ross, J. T. Gostick, Q. Liu, *J. Appl. Electrochem.* **2011**, *41*, 1137.

[26] Y. Liu, S. Lu, S. Chen, H. Wang, J. Zhang, Y. Xiang, *ACS Appl. Mater. Interfaces* **2019**, *2*, 2469.

[27] N. Nitta, F. Wu, J. T. Lee, G. Yushin, *Mater. Today* **2015**, *18*, 252.

[28] A. Seidel, J. J. Waypa, M. Elimelech, *Energy Environ. Sci.* **2001**, *18*, 105.

[29] M. J. Frisch, G. W. Trucks, H. B. Schlegel, G. E. Scuseria, M. A. Robb, J. R. Cheeseman, G. Scalmani, V. Barone, B. Mennucci, G. A. Petersson, H. Nakatsuji, M. Caricato, X. Li, H. P. Hratchian, A. F. Izmaylov, J. Bloino, G. Zheng, J. L. Sonnenberg, M. Hada, M. Ehara, K. Toyota, R. Fukuda, J. Hasegawa, M. Ishida, T. Nakajima, Y. Honda, O. Kitao, H. Nakai, T. Vreven, J. A. Montgomery, Jr., J. E. Peralta, F. Ogliaro, M. Bearpark, J. J. Heyd, E. Brothers, K. N. Kudin, V. N. Staroverov, T. Keith, R. Kobayashi, J. Normand, K. Raghavachari, A. Rendell, J. C. Burant, S. S. Iyengar, J. Tomasi, M. Cossi, N. Rega, J. M. Millam, M. Klene, J. E. Knox, J. B. Cross, V. Bakken, C. Adamo, J. Jaramillo, R. Gomperts, R. E. Stratmann, O. Yazyev, A. J. Austin, R. Cammi, C. Pomelli, J. W. Ochterski, R. L. Martin, K. Morokuma, V. G. Zakrzewski, G. A. Voth, P. Salvador, J. J. Dannenberg, S. Dapprich, A. D. Daniels, O. Farkas, J. B. Foresman, J. V. Ortiz, J. Cioslowski, D. J. Fox, Gaussian 09, Revision E.01, Gaussian, Inc., Wallingford CT, **2013**.

Manuscript received: May 20, 2020
Revised manuscript received: June 23, 2020
Accepted manuscript online: July 13, 2020
Version of record online: July 29, 2020